# Non-uniform local interpolatory subdivision surfaces for regular quadrilateral meshes

Carolina Vittoria Beccari[a,*], Giulio Casciola[a], Lucia Romani[b]

[a]*Department of Mathematics, University of Bologna, P.zza Porta San Donato 5, 40127 Bologna, Italy*
[b]*Department of Mathematics and Applications, University of Milano-Bicocca, Via R. Cozzi 53, 20125 Milano, Italy*

**Abstract**

Subdivision is a powerful mechanism for generating curves and surfaces from discrete sets of control points. So far, the main advantage of subdivision methods with respect to other free-form representations, such as splines, has been acknowledged in their ability to generate smooth surfaces of arbitrary topology. In this paper we propose a method to generate non uniform subdivision surfaces interpolating regular quadrilateral meshes. We show that, choosing a suitable parameterization and properly setting edge and face point rules, these surfaces favorable compare both with their uniform counterpart and with non uniform tensor product splines.

*Keywords:* Interpolation, Non-uniform parameterization, Subdivision surfaces

## 1. Introduction

In this paper we consider the problem of interpolating a regular grid of points, i.e. a quadrilateral net where each vertex has four incident edges. The easiest approach relies on parametric tensor-product surfaces and, since the ability to control the final shape is fundamental in a variety of applications, a crucial issue is how to suitably choose the parameter values corresponding to the interpolation points. The parameterization, in fact, significantly affects the visual appearance of the interpolant. While in the surface case investigations on this topic are still very limited, in the curve case several results have already been collected. In particular, it is well known that, when interpolating unequally spaced data, the uniform parameterization corresponds to the most unsatisfactory choice since it tends to create artifacts such as cusps and self-intersections; oppositely, the centripetal parameterization leads to curves that favorably compare with their uniform counterpart, as they stay closer to the assigned polyline. An example of the different behavior of the same interpolant with respect to uniform and centripetal parameterization is given in Figure 1, exploiting the class of locally supported spline functions proposed in [5].

For many years, the reasoning behind the conjecture that the centripetal parameterization be optimal in the context of interpolation has been limited to informal explanations based on intuition. Only recently the work in [10] has provided a formal mathematical explanation of the fact that, for cubic splines, the centripetal parameterization significantly bounds the global and local deviation of the resulting curve from its data polygon. In a similar way, in [18], it is proven that, for cubic Catmull-Rom curves, the centripetal parameterization is the only one that guarantees no cusps and self-intersections within curve segments. As concerns interpolating subdivision curves, a result confirming the advantage of the centripetal parameterization was proven in [7] where, for the 4-point scheme, the uniform, chordal and centripetal parameterizations are compared, showing that the centripetal one minimizes the distance between data polygon and limit curve.

For all these reasons, it is natural to consider the centripetal parameterization the best choice within the family of non-uniform parameterizations also in the surface case, when using a tensor-product spline to interpolate the vertices of a quadrilateral mesh.

*Corresponding author.
*Email addresses:* beccari@dm.unibo.it (Carolina Vittoria Beccari), casciola@dm.unibo.it (Giulio Casciola), lucia.romani@unimib.it (Lucia Romani)

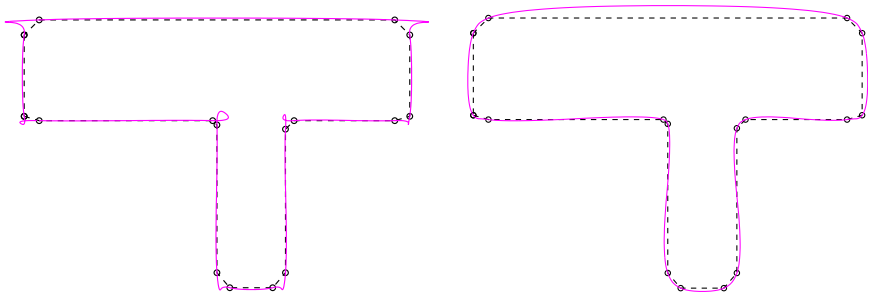

Figure 1: Comparison between quadratic spline curves interpolating highly non-uniform data through uniform (left) and centripetal (right) parameterization.

This work originates from the observation that, even if based on the centripetal parameterization, a tensor-product spline interpolant may not offer an optimal solution to the considered interpolation problem. To understand why, let us denote by $\mathcal{P} = \{p_{i,j}\}_{i,j\in\mathbb{Z}}$ the vertices of the given regular quadrilateral mesh and by $\mathcal{X} = \{x_{i,j}\}$ the associated non-uniform parameter values. In order to compute the tensor-product surface interpolating the vertices $p_{i,j}$ in correspondence to the parameters $x_{i,j}$, it is necessary to work out only two parameter sets corresponding to the axial directions. The solving strategy is to compute the average of the parameter values $x_{i,j}$, previously defined along the two directions, thus loosing information that turn out to be crucial to the quality of the interpolant. In particular each section curve of the mesh is not allowed to maintain its own non-uniform parameterization, as would be especially desirable in the interpolation context, but it is parameterized by the average of the parameterizations of all section curves in the related axial direction. The strict structure of the tensor product is thus acknowledged as the main obstacle to a good interpolant, as discussed e.g. in [9], §7.5.1.
In the remainder of the paper we introduce a novel method to get a good quality surface interpolating the vertices of a regular quadrilateral mesh, by defining a non-uniform interpolatory subdivision algorithm that exploits the advantages of a whole set of parameters $x_{i,j}$.
For approximation purposes, similar methods were firstly studied in [14] and most recently in [3, 13], where the authors propose non-uniform subdivision algorithms based on biquadratic and bicubic B-splines. In this paper we will focus our attention on the problem of interpolating quadrilateral nets through non-uniform refinement rules based on a class of univariate interpolatory 4-point schemes. In the context of interpolatory subdivision, univariate refinement algorithms with non-uniform parameters were firstly introduced by Daubechies et al. [6]. Dyn et al. [7] successively proposed to apply iterated centripetal parameterizations to the 4-point scheme of this family derived by up-sampling from the cubic non-uniform Lagrange interpolant. Since this approach requires recomputing the underlying parameterization at each subdivision step, the resulting refinement process is non-linear and, by using an ad hoc analysis, the authors prove that it generates $C^0$ limit curves.
In this paper we provide the general refinement rules of a non-uniform 4-point based subdivision algorithm that, besides exploiting the advantages of the centripetal parameterization, is linear and capable of generating continuous surfaces of good quality. Due to the acknowledged difficulty of the problem, $G^1$ continuity is only conjectured and empirically shown by a wide range of experiments.

The remainder of the paper is organized as follows. In Section 2 we recall the refinement rules of the class of non-uniform interpolatory 4-point schemes we start with. In Section 3 we describe the key ideas at the basis of our non-uniform interpolatory subdivision scheme for regular quadrilateral meshes and we explain in detail the edge and face point rules it relies upon. Then, in Section 4 we perform the continuity analysis of the proposed surface scheme and in Section 5 we show some numerical examples confirming the effectiveness of our proposal and its advantages with respect to its uniform counterpart and to tensor-product splines. A summary of the main contributions of this paper and the outline of our future work are described in Section 6.

## 2. A class of non-uniform interpolatory 4-point schemes

The novel surface scheme we are going to present is conceived as a generalization of a non-uniform interpolatory 4-point scheme, that we will call *reference scheme*. Thus, before defining the surface refinement rules, we briefly overview the related univariate method.
Denoted by $\mathcal{P}^0 = \{p_i^0\}$ the vertices of the initial polyline and by $\mathcal{X}^0 = \{x_i^0\}$ the associated parameterization, for all $k \geq 0$ the general form of the refinement equations of a non-uniform interpolatory 4-point scheme is

$$\begin{aligned} p_{2i}^{k+1} &= p_i^k \\ p_{2i+1}^{k+1} &= a_{0,i}^k p_{i-1}^k + a_{1,i}^k p_i^k + a_{2,i}^k p_{i+1}^k + a_{3,i}^k p_{i+2}^k \end{aligned}$$

where the coefficients $a_{h,i}^k$, $h = 0, ..., 3$ strictly depend on the parameterization of the $k$-level polyline $\mathcal{P}^k$. It is natural to assume that these coefficients depend on the length of the three consecutive knot intervals $d_j^k := x_{j+1}^k - x_j^k$, $j = i-1, i, i+1$ and thus we can conveniently denote them as $a_{h,i}^k$ or

$$a_h(d_{i-1}^k, d_i^k, d_{i+1}^k), \quad h = 0, ..., 3.$$

Notice that the two notations are equivalent when we have a sequence of parameters - as it is in this section - that are indexed by subsequent integers. In general a subsequent labeling of parameters is not always possible or convenient on a mesh (as we will see in the following section), thus we will use the second notation where it will be necessary to explicitly specify the three knot intervals involved in the definition of the refinement coefficients.
The quadruple of coefficients that defines the reference scheme can be easily obtained by fitting a local function, supported on three intervals, through the points $(x_h^k, p_h^k)$, $h = 0, ..., 3$ and evaluating it at an arbitrary parameter value inside the central interval $[x_i^k, x_{i+1}^k]$. As a consequence any possible choice of local interpolant gives rise to a different coefficients set, so that a large number of subdivision schemes fitting into the considered framework is available.
From this point onward we will restrict our attention to the category of the so called *semi-regular* insertion rules, where the coefficients $a_{h,i}^k$, $h = 0, ..., 3$, are obtained by evaluating the locally fitted interpolant at the parameter value $(x_i^k + x_{i+1}^k)/2$. In this way, if we use non-uniform cubic Lagrange interpolation, the derived coefficients are

$$\begin{aligned} a_0(d_{i-1}^k, d_i^k, d_{i+1}^k) &= -\frac{(d_i^k)^2(d_i^k + 2d_{i+1}^k)}{8d_{i-1}^k(d_{i-1}^k + d_i^k)(d_{i-1}^k + d_i^k + d_{i+1}^k)} \\ a_1(d_{i-1}^k, d_i^k, d_{i+1}^k) &= \frac{(d_i^k)^2 + 2(d_{i-1}^k + d_{i+1}^k)d_i^k + 4d_{i-1}^k d_{i+1}^k}{8d_{i-1}^k(d_i^k + d_{i+1}^k)} \\ a_2(d_{i-1}^k, d_i^k, d_{i+1}^k) &= \frac{(d_i^k)^2 + 2(d_{i-1}^k + d_{i+1}^k)d_i^k + 4d_{i-1}^k d_{i+1}^k}{8d_{i+1}^k(d_{i-1}^k + d_i^k)} \\ a_3(d_{i-1}^k, d_i^k, d_{i+1}^k) &= -\frac{(d_i^k)^2(2d_{i-1}^k + d_i^k)}{8d_{i+1}^k(d_i^k + d_{i+1}^k)(d_{i-1}^k + d_i^k + d_{i+1}^k)} \end{aligned} \tag{1}$$

while if we interpolate through the non-uniform quadratic cardinal splines in [5] we obtain

$$\begin{aligned} a_0(d_{i-1}^k, d_i^k, d_{i+1}^k) &= -\frac{(d_i^k)^2}{8d_{i-1}^k(d_{i-1}^k + d_i^k)} \\ a_1(d_{i-1}^k, d_i^k, d_{i+1}^k) &= \frac{(d_i^k)^2 + d_i^k(3d_{i-1}^k + d_{i+1}^k) + 4d_{i-1}^k d_{i+1}^k}{8d_{i-1}^k(d_i^k + d_{i+1}^k)} \\ a_2(d_{i-1}^k, d_i^k, d_{i+1}^k) &= \frac{(d_i^k)^2 + d_i^k(d_{i-1}^k + 3d_{i+1}^k) + 4d_{i-1}^k d_{i+1}^k}{8d_{i+1}^k(d_i + d_{i-1})} \\ a_3(d_{i-1}^k, d_i^k, d_{i+1}^k) &= -\frac{(d_i^k)^2}{8d_{i+1}^k(d_i^k + d_{i+1}^k)}. \end{aligned} \tag{2}$$

The above schemes provide a couple of examples of coefficients that have been proved to generate $C^1$ continuous limit curves (see [7] and [1], respectively).
Before moving to the description of the surface method, it is important to point out that the reader may assume as a starting point for the surface subdivision algorithm described in the next section any suitable univariate non-uniform 4-point scheme. There are only two requirements that the chosen scheme should fulfill, namely

- The coefficients $a^k_{h,i}$ depend on the parameters of the three edges involved in the insertion process, i.e. they can be written as $a_h(d^k_{i-1}, d^k_i, d^k_{i+1})$;
- The scheme guarantees at least $C^0$ continuous limit curves.

## 3. The Non-Uniform Local Interpolatory Subdivision Scheme (NULISS) for regular quadrilateral meshes

The existing literature has always considered subdivision schemes as advantageous alternatives to tensor-product constructions due to their ability to deal with extraordinary points and model surfaces of arbitrary topology. Conversely, in this paper, we want to point out that subdivision can perform significantly better than tensor-product splines also in the context of interpolation of regular quadrilateral meshes. The goal of this section is to provide a general formulation of a 4-point based interpolatory subdivision scheme for regular (i.e. valence 4) quadrilateral meshes that offers a very efficient tool for interpolating a given net of points taking into account the associated parameter values. Hereinafter this scheme will be called NULISS (Non-Uniform Local Interpolatory Subdivision Scheme). Its insertion rules are conceived as a natural extension to the regular quadrilateral mesh of a non-uniform interpolatory 4-point scheme with the requirements stated in Section 2.
Let $\mathcal{M}^0$ denote the initial mesh, i.e. the initial polyhedron-like configuration of faces, edges and vertices such that each vertex corresponds to a point in 3D space, each edge is a line segment bounded by two vertices, and each face is bounded by a loop of four edges. We also require that each edge is shared exactly by two faces (except for boundary edges which belong to one face only) and in each loop adjacent edges share a vertex. Denoted by $\mathcal{P} = \{p_{i,j}\}_{i,j\in\mathbb{Z}}$ the vertices of the mesh and by $\mathcal{X} = \{x_{i,j}\}$ the related non-uniform parameter values, we associate with each edge along the horizontal axial direction a knot interval $d^0_{i,j} = \|p^0_{i+1,j} - p^0_{i,j}\|_2^{\frac{1}{2}}$, according to the centripetal parameterization. Analogously, along the other direction, we will define knot intervals $e^0_{i,j} = \|p^0_{i,j+1} - p^0_{i,j}\|_2^{\frac{1}{2}}$. Reasoning in terms of parameters or of the associated knot intervals is clearly equivalent, however, for the sake of computational simplicity, it turns out to be more convenient to express the insertion rules depending on the knot intervals $d^0_{i,j}$ and $e^0_{i,j}$. Thus, the subdivision algorithm we are going to propose takes as input the mesh $\mathcal{M}^0$ with the associated initial knot intervals and generates a smooth surface as the limit of the process of recursive refinement. At each iteration, the process follows the steps outlined below.

**Algorithm 1.** *For each $k \geq 1$, it*

1. *retains each vertex point (Figure 2-left, green bullets);*
2. *computes a new edge point for each edge (Figure 2-left, magenta bullets);*
3. *computes a new face point for each face (Figure 2-left, blue bullets);*
4. *creates new edges by connecting each new face point to the new edge points of the edges surrounding the face, and connecting each vertex point to the new edge points of the edges incident on that vertex;*
5. *creates new faces that have a loop of four new edges;*
6. *computes the knot interval values for the refined mesh and assigns them to the new edges.*

The above steps 1.,2.,3. define the new geometry and steps 4., 5. define the connectivity. When this process step continues, it yields a sequence of refined meshes which converges to a limit surface.
Vertex, edge and face points are determined by the equations

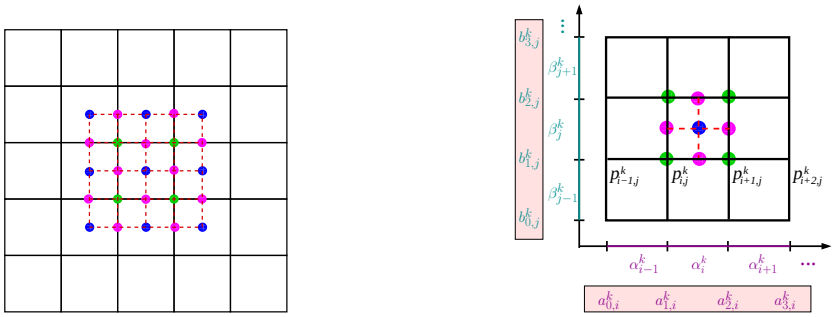

Figure 2: Left: One step of the proposed interpolatory subdivision algorithm, the initial mesh is in black, while the refined mesh in red. Green, magenta and blue bullets represent respectively vertex, edge and face points. Right: Parameters configuration and related coefficients for the tensor product scheme.

- vertex points $p^{k+1}_{2i,2j} = p^k_{i,j}$;
- edge points $p^{k+1}_{2i+1,2j} = \sum_{h=0}^{3} a^k_{h,i}\, p^k_{i+h-1,j}$ and $p^{k+1}_{2i,2j+1} = \sum_{\ell=0}^{3} b^k_{\ell,j}\, p^k_{i,j+\ell-1}$;
- face points $p^{k+1}_{2i+1,2j+1} = \sum_{h=0}^{3}\sum_{\ell=0}^{3} a^k_{h,i}\, b^k_{\ell,j}\, p^k_{i+h-1,j+\ell-1}$.

As previously mentioned, in the tensor-product case we need to define an average parameterization where

$$\alpha^k_i = \frac{\sum_{j\in\mathbb{Z}} d^k_{i,j}}{\sharp\{d^k_{i,j} |\ j \in \mathbb{Z}\}} \quad \text{and} \quad \beta^k_j = \frac{\sum_{i\in\mathbb{Z}} e^k_{i,j}}{\sharp\{e^k_{i,j} |\ i \in \mathbb{Z}\}},$$

so that $\{\alpha^k_i\}_{i\in\mathbb{Z}}$ and $\{\beta^k_j\}_{j\in\mathbb{Z}}$ are the knot intervals associated with the two axial directions (see Figure 2-right for a graphical interpretation). Thus, in the notation introduced in Section 2, the coefficients $a^k_{h,i}$ and $b^k_{\ell,j}$ can be written as $a^k_{h,i} = a_h(\alpha^k_{i-1}, \alpha^k_i, \alpha^k_{i+1})$ and $b^k_{\ell,j} = a_\ell(\beta^k_{j-1}, \beta^k_j, \beta^k_{j+1})$, $h, \ell = 0, ..., 3$ and are determined by the chosen univariate subdivision scheme.

As previously discussed, the requirement for averaging the parameterization may determine a significant loss of quality in the limit surface. Our goal is thus to generalize the above edge and face point formulas so as to consider a whole set of parameters surrounding the location of insertion.

If we focus our attention on the neighborhood of a vertex $p^k_{i,j}$ of the mesh $\mathcal{M}^k$ (produced after $k$ refinements), it is evident that the configuration of faces and vertices around this point has rotational symmetry and remains topologically invariant through refinement. Thus, from this point onward, we will use the indexing scheme illustrated in Figure 3, where points and parameters are partitioned into 4 sectors, that reflect the local structure of the mesh. In particular, to write the refinement equations of the scheme in the non tensor-product case, 12 vertices and 6 parameters per each sector are needed. As it will be clear in the following section, this labeling strategy turns out to be the most convenient when analyzing the continuity of the limit surface.

In the new notation, the vertex $p^k_{i,j}$ is now indicated as $p^k_0$ and it is obviously a fixed point of the refinement process, thus $p^0_0 = p^k_0$, $\forall k \geq 1$. In order to describe the refinement rules of our new proposal, it is sufficient to focus on one of the four faces meeting at $p^k_0$, so we can choose the face corresponding to the first sector, that is determined by vertices $p^k_0$, $p^k_1$, $p^k_2$ and $p^k_{37}$. For this face, we need to properly define steps 2. and 3. of our algorithm. Due to rotational symmetry, formulas for the other edge and face points can be computed analogously.

The refinement process is illustrated in Figure 4. For any $s = 1, ..., 4$, that identifies one of the sectors around the given vertex, we define the triple of knot intervals

$$\epsilon^k_s = \{d^k_{j+12}, d^k_j, d^k_{j+1}\}, \qquad j = 1 + 6(s-1),$$

where the indices $j$ are cyclic of period 24. A new edge point $E^{k+1}_1$ is placed in the middle of the edge $p^k_0, p^k_1$ by the formula

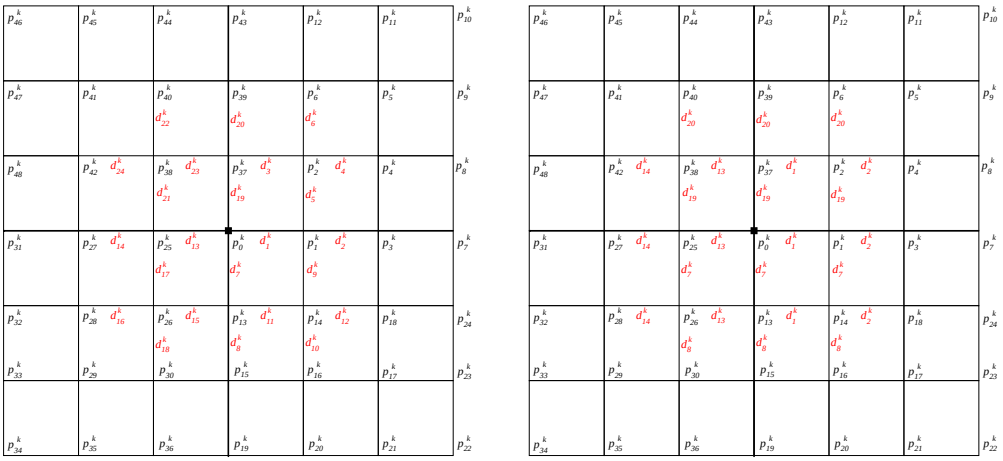

Figure 3: Left: indexing of points and parameters at refinement level $k$. Right: configuration of parameters in the tensor-product case.

$$E_1^{k+1} = a_0(\epsilon_1^k)\, p_{25}^k + a_1(\epsilon_1^k)\, p_0^k + a_2(\epsilon_1^k)\, p_1^k + a_3(\epsilon_1^k)\, p_3^k \tag{3}$$

where coefficients $a_h(\epsilon_1^k)$, $h = 0, ..., 3$, are computed as described in Section 2; this means that the new edge point is generated by applying the insertion rule of the chosen univariate reference scheme to the related edge of $\mathcal{M}^k$ (see Figure 4-left). The edge points along the other edges can be determined following a similar approach.

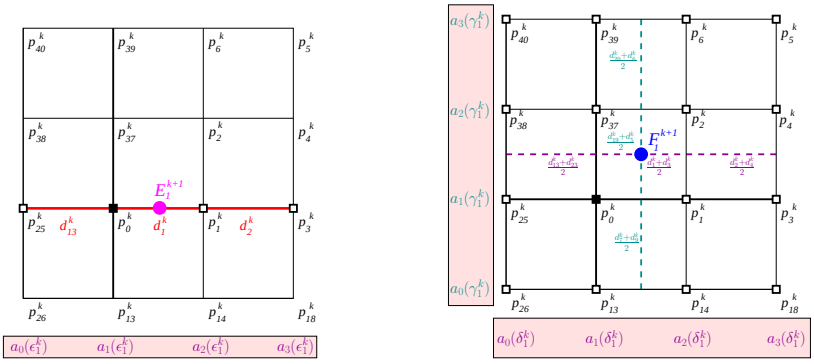

Figure 4: Edge point rule (left) and face point rule (right) for the first sector.

To explain the insertion of a face point we observe that the vertices of the face of insertion can be seen as the intersection of 4 section curves, two in each direction. Since the scheme is interpolatory, the section curves whose intersections determine the face are the limit of corresponding polylines of the current mesh. At this stage, it is convenient to introduce some further notation. For each sector $s = 1, ..., 4$ we define

$$\delta_s^k = \left\{ \frac{d_{j+12}^k + d_{j+22}^k}{2}, \frac{d_j^k + d_{j+2}^k}{2}, \frac{d_{j+1}^k + d_{j+3}^k}{2} \right\} \quad \text{and} \quad \gamma_s^k = \left\{ \frac{d_{j+6}^k + d_{j+8}^k}{2}, \frac{d_{j+18}^k + d_{j+4}^k}{2}, \frac{d_{j+19}^k + d_{j+5}^k}{2} \right\},$$

with $j = 1 + 6(s-1)$. For the sake of simplicity, if we focus on the first sector, $\delta_1^k$ and $\gamma_1^k$ are length-3 sequences of knot intervals that refer to *virtual* edges (i.e. edges that do not appear in the coarse mesh) and they are computed

by averaging existing knot intervals on opposite edges of the considered face and of the adjacent faces. They can be respectively seen as the parameterization of two virtual section curves, each of them located between the two section curves that determine the face in each direction. We can now compute $a_h(\delta_1^k)$ and $a_h(\gamma_1^k)$, $h = 0, ..., 3$ and determine the location of one of the face points as

$$\begin{aligned} F_1^{k+1} &= a_0(\gamma_1^k)(a_0(\delta_1^k)p_{26}^k + a_1(\delta_1^k)p_{13}^k + a_2(\delta_1^k)p_{14}^k + a_3(\delta_1^k)p_{18}^k) \\ &+ a_1(\gamma_1^k)(a_0(\delta_1^k)p_{25}^k + a_1(\delta_1^k)p_0^k + a_2(\delta_1^k)p_1^k + a_3(\delta_1^k)p_3^k) \\ &+ a_2(\gamma_1^k)(a_0(\delta_1^k)p_{38}^k + a_1(\delta_1^k)p_{37}^k + a_2(\delta_1^k)p_2^k + a_3(\delta_1^k)p_4^k) \\ &+ a_3(\gamma_1^k)(a_0(\delta_1^k)p_{40}^k + a_1(\delta_1^k)p_{39}^k + a_2(\delta_1^k)p_6^k + a_3(\delta_1^k)p_5^k). \end{aligned} \tag{4}$$

Figure 4-right illustrates the insertion method for such a face point.

**Remark 1.** *Note that whenever initial knot intervals are set up compatibly with the tensor-product structure (that is the same parameter value is assigned to each row and column of the mesh), the NULISS scheme exactly coincides with the tensor-product of the univariate 4-point scheme recalled in Section 2.*

**Remark 2.** *The proposed face point insertion rule does not involve the complete set of parameters associated with the 4 × 4 grid of vertices that determines a new face point. Based on our numerical experiments, we found better results by considering only the parameters of the vertices related to the face of insertion and to the adjacent faces. In fact, it makes sense to require that the virtual parameterization adopted to insert a face point, does not significantly deviate from the parameterization of the section curves that define a face. Conversely taking into account the whole 4 × 4 grid of parameters may generate undesired distortions in the parameterization.*

**Remark 3.** *Oppositely to the tensor-product construction, the edge point rules of the proposed scheme ensure that the vertices that describe each section polyline of the mesh are interpolated at the corresponding centripetal parameters. In this way, each section curve of the limit surface maintains its own parameterization (instead of being parameterized by the average of the parameterizations in the related axial direction) and thus it has the optimal visual quality guaranteed by the centripetal parameterization.*

So far we have described steps 1.-5. in Algorithm 1. The following subsection illustrates the strategy that we found most convenient to accomplish step 6 of the proposed subdivision algorithm.

### *3.1. Parameters updating*

Each subdivision step generates a refined mesh, with more vertices, edges and faces, and as a consequence a suitable parameterization should be set in correspondence to the newly created vertices. The method that we choose to compute the values of the knot-intervals influences the linearity and stationarity of the scheme as well as the properties of the limit shape, thus it should be carefully devised. Before illustrating our proposal, we want to point out that one natural possibility would be to recompute the centripetal parameterization at each level of refinement. However this strategy is very expensive from a computational viewpoint and does not offer any remarkable advantage, due to the fact that the visual appearance of the limit surface is established during the first refinement steps. Furthermore, recomputing the parameterization gives rise to a non-linear and non-stationary process, which constitutes a big down point, since the analysis of the resulting scheme is extremely difficult.
For all these reasons, in order to guarantee that the refinement rules identify a linear subdivision process, we will use an updating strategy to deduce the $k$-level knot intervals from those computed at level 0. In particular, for all $k > 0$, the knot intervals defined in correspondence to edges of the coarse mesh will be duplicated, while those in correspondence to a new edge created inside a face will be obtained by averaging knot intervals on the opposite edges of that face, as shown in Figure 5 for two successive refinement steps. In this way the $k$-level parameter values are expressed by the updating formulas

$$
\begin{aligned}
d_j^k &= d_j^0, \\
d_{j+1}^k &= d_{j+1}^0, \\
d_{j+2}^k &= \left(1-\frac{1}{2^k}\right) d_j^0 + \frac{1}{2^k} d_{j+2}^0, \\
d_{j+3}^k &= \left(1-\frac{1}{2^k}\right) d_j^0 + \frac{1}{2^k} d_{j+3}^0, \\
d_{j+4}^k &= \left(1-\frac{1}{2^k}\right) d_{j+18}^0 + \frac{1}{2^k} d_{j+4}^0, \\
d_{j+5}^k &= \left(1-\frac{1}{2^k}\right) d_{j+18}^0 + \frac{1}{2^k} d_{j+5}^0
\end{aligned}
\tag{5}
$$

with $j = 1+6(s-1)$, $s = 1, ..., 4$ (the indices $j$ should be intended cyclic of period 24), assuming that at each refinement a new knot is inserted in correspondence to the mid-point of each parameter interval.
Although there are clearly many available methods for computing the new parameters, the strategy that we have chosen turns out to be crucial when performing the continuity analysis of the subdivision scheme, as it will be evident in the next section.

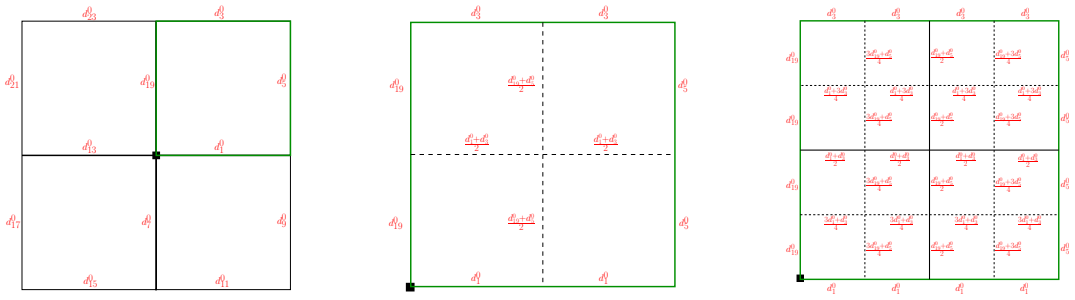

Figure 5: Knot intervals for the initial configuration ($k = 0$) around the vertex $p_0^0$ (left). Knot intervals of the first sector at refinement level $k = 1$ (center) and $k = 2$ (right).

## 4. Continuity analysis

The aim of this section is to provide an analysis algorithm for the non-uniform surface scheme considered in this paper. We remark that, since the scheme is both non-stationary and non-uniform, it is not possible to exploit the available analysis tools for non-stationary schemes, like the well-established method of asymptotical equivalence [8], or the most recent results based on the idea of proximity [11, 15, 16]. Thus we will follow a different approach that strongly relies on the chosen parameters updating strategy. In particular, we will prove that, whenever the parameters are computed through relation (5), any subdivision scheme originated by a reference scheme that satisfies the requirements fixed in Section 2 generates continuous limit surfaces, independently of the initial parameters configuration.

### *4.1. Structure of the limit surface*

To analyze the continuity of the scheme, it is fundamental to understand how the parameters along the edges in the considered neighborhood evolve through subsequent refinements and how their behavior affects the structure of the limit surface. Figure 5-left schematically presents the initial setting of parameters on the four faces meeting at $p_0^0$

and their values after the first two refinement steps (Figure 5 center and right, respectively). During all the subsequent steps, the configuration of parameters evolves analogously, so it is straightforward to figure out the parameters configuration at any level $k > 2$. In particular, after two steps of the subdivision algorithm three different kinds of regions are identified (see Figure 6), which we refer to as:

1. *Tensor-product regions*, where parameters on each row and column can be scaled to the same value;
2. *Regions augmented across one edge*, where either parameters on each column or row can be scaled to the same value;
3. *Regions augmented around a vertex*, where there is no possible scaling that brings back the knot intervals to the same values either on each column or row.

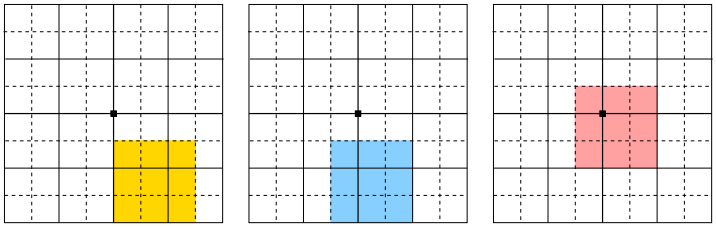

Figure 6: The three different types of regions obtained after two subdivision steps: tensor-product region (left), region augmented across one edge (center), region augmented around a vertex (right).

In the sequel we discuss the behavior of the mesh through successive refinement levels and in the different regions, and, as a consequence, how the three cases above should be treated when analyzing the convergence of the scheme.

*Tensor-product regions.* The local configuration of parameters inside these regions implies that, when the parameters are substituted in the refinement equations of the scheme, the positions of the new vertices in or on the boundary of these regions, are exactly the same as if all the horizontal intervals had been equal and all the vertical intervals equal likewise. Thus, in these regions, the scheme converges to the tensor-product surface generated by a $C^0$, uniform, 4-point scheme. As a consequence the limit surface is trivially $C^0$. Moreover, if the univariate reference scheme generates $C^1$ continuous limit curves, the limit surface inside these regions will be $C^1$ continuous as well.

*Regions augmented across one edge.* The situation across edges of augmented faces can be seen as a special case of the third kind of regions, that are augmented around a vertex. Therefore the analysis of continuity can be addressed as in the more general case of vertices between augmented faces.

*Regions augmented around a vertex.* We say that a vertex is *augmented* if, in its neighborhood, the parameterization of the mesh is non-uniform and does not have a tensor-product structure. Thus, to prove convergence of the scheme at a given augmented vertex $p_0^0$, we will show that, independently of the underlying parameterization, any arbitrary initial configuration of points converges to $p_0^0$. Before going into the details of our analysis, we observe that, proving that all points in the neighborhood of an initial vertex converge to that vertex does not only imply pointwise convergence, but also continuity of the limit surface. To understand why, we shall keep track of how the parameterization of the four initial faces meeting at the augmented vertex $p_0^0$ evolves through successive iterations. In particular, recalling relations (5), it can be easily seen that, after a few subdivision steps, the parameters configuration is such that, up to proper rescaling, a tensor-product region arises in the interior of each of the four initial faces. We denote this region as $T_s^k$, $s = 1, ..., 4$, since its extension depends on the subdivision level $k$ (see Figure 7). From the $k$-th refinement step onward, the points generated by the NULISS scheme inside the region $T_s^k$ can be equivalently generated by applying the tensor-product scheme of the uniform 4-point subdivision scheme. Thus, in these regions, the regularity of the limit surface is guaranteed by the properties of the univariate scheme.
In the region surrounding the boundary of the four initial faces, we have a strip of augmented faces, whose parameters cannot be suitably rescaled to fit the definition of tensor-product. If all the initial points in the 3-ring of $p_0^0$ converge to $p_0^0$, the tensor-product area extends to the boundary of each initial face and tends to cover the whole face area,

while at each iteration the augmented strip shrinks, approximately halving its width. Moreover, by construction of the scheme, the limit surface patches associated with neighboring initial faces have a common boundary, since their boundary curves are limit curves of the non-uniform univariate scheme. As a consequence, if all the initial points in the 3-ring of $p_0^0$ converge to $p_0^0$, the subdivision process generates a continuous limit surface.

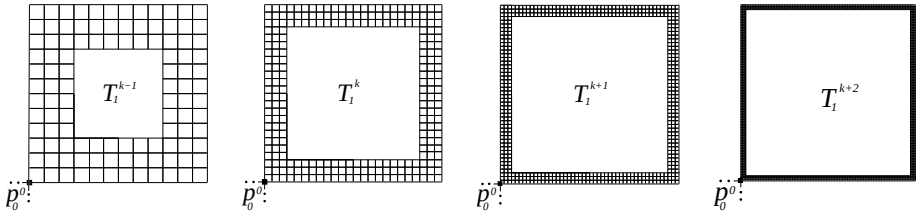


Figure 7: Evolution through 4 subsequent refinement steps of the tensor-product region inside one face containing $p_0^0$.

*4.2. The local subdivision matrix*

As the support of the subdivision scheme is of width 6 and symmetric with respect to $p_0^0$, we can restrict our analysis to the three rings of vertices surrounding $p_0^0$ [19]. The points in the 3-neighborhood of $p_0^0$ are partitioned into 4 sectors, where each sector is associated with an index $s = 1, ..., 4$. More precisely, at refinement level 0 we denote by $P_s^0$ the vector of points $P_s^0 := [p_{12(s-1)+1}^0, p_{12(s-1)+2}^0, \cdots, p_{12(s-1)+12}^0]$, with $s = 1, ..., 4$. The subdivision process can now be formalized as

$$P^{k+1} = M^k P^k, \quad \text{where} \quad P^k := [p_0^0, P_1^k, P_2^k, P_3^k, P_4^k]^T, \quad \forall k \geq 0. \tag{6}$$

Since the scheme is interpolatory, the point $p_0^0$ is a fixed point of the iterative process (6). The matrix $M^k$, that maps the points from refinement level $k$ to $k+1$ represents the refinement rules of the scheme, where the coefficients of $M^k$ depend on the local parameterization associated with $k$-level edges.
Moreover, from the updating formulas (5) we can easily see that, after two iterations of the scheme, the entries of the subdivision matrix $M^k$ depend only on the initial parameterization of the first ring of vertices around $p_0^0$; in this way, for any level $k \geq 2$, the initial parameters involved in the subdivision process turn out to be $d_j^0$, $d_{j+2}^0$, $d_{j+4}^0$, $j = 1 + 6(s-1)$, with $s = 1, ..., 4$. It is therefore sufficient to analyze the convergence of the subdivision process starting from the 2-nd refined control net.

**Remark 4.** *Recalling the parameters updating equations* (5)*, it can be easily observed that the entries of the infinite sequence of matrices $M^0 = [m_{i,j}^0]$, $M^1 = [m_{i,j}^1]$, ..., that defines the subdivision process* (6)*, converge as $k$ tends to infinity, i.e.*

$$\lim_{k\to\infty} m_{i,j}^k = m_{i,j}$$

*and in particular the sequence $\{M^k\}_{k>0}$ converges to a matrix $M$ whose entries are given by the tensor-product of the univariate schemes along the two directions that intersect at $p_0^0$. Due to our parameters updating method, from the second iteration of the scheme onward, the entries of the limit matrix $M = [m_{i,j}]$, $i, j = 1, ..., 49$, can thus be obtained by substituting into relations* (1) *or* (2) *the sequences of parameters ..., $d_{13}^0, d_{13}^0, d_1^0, d_1^0$, ... in the horizontal grid direction and ..., $d_7^0, d_7^0, d_{19}^0, d_{19}^0$, ... in the vertical one, that are piecewise uniform around $p_0^0$.*

Moreover, for any level $k$, the subdivision matrix related to the 3-neighborhood of $p_0^0$ has the structure

$$M^k = \begin{bmatrix} 1 & 0 & 0 & 0 & 0 \\ \nu^k(1) & B_1^k(1) & B_2^k(1) & B_3^k(1) & B_4^k(1) \\ \nu^k(2) & B_4^k(2) & B_1^k(2) & B_2^k(2) & B_3^k(2) \\ \nu^k(3) & B_3^k(3) & B_4^k(3) & B_1^k(3) & B_2^k(3) \\ \nu^k(4) & B_2^k(4) & B_3^k(4) & B_4^k(4) & B_1^k(4) \end{bmatrix}. \tag{7}$$

where the blocks $\nu^k(s)$ and $B_i^k(s)$ are respectively $12 \times 1$ and $12 \times 12$ real matrices, whose entries depend on the sector $s = 1, ..., 4$ and can be derived by the refinement rules (3) and (4).

**Remark 5.** *If the parameterization is uniform, the matrix obtained by removing the first row and column of $M^k$ is block circulant. Oppositely, in the case of the NULISS scheme, the entries of each block of $M^k$ depend on the local parameterization of each sector, thus we do not have this circulant structure.*

*4.3. Continuity around an augmented vertex*

We can now exploit the local subdivision matrices $M^k$, $k = 2, 3, ...$ to prove convergence of the scheme in the neighborhood of the augmented vertex $p_0^0$. As pointed out in the previous section, for the proposed scheme, convergence also implies continuity of the limit surface.
In particular, any subdivision scheme of the kind considered in the previous section is convergent if the following three statements hold:

1. The sequence $\{M^k\}_{k>0}$ converges to $M$;
2. Each matrix $M^k$ is non expansive;
3. The only fixed point of $M$ is $p_0^0$.

Items 1. to 3. provide an analysis algorithm that we can apply to any subdivision scheme to verify its convergence. In the following we will show that these three steps imply the convergence of the subdivision scheme.

Let $\|\quad\|$ a vector norm in $\mathbb{C}^n$. We introduce the following definition.

**Definition 1.** *A matrix $S \in \mathbb{C}^{n\times n}$ is* nonexpansive *with respect to $\|\quad\|$ if for any $x \in \mathbb{C}^n$*

$$\|Sx\| \leq \|x\|.$$

Moreover the following result holds true, which is a generalization of the well known theory on matrix analysis (cfr. [12], Sections 5.6.9 - 5.6.12).

**Theorem 1.** *A matrix $S \in \mathbb{C}^{n\times n}$ is non expansive with respect to a matrix norm on $\mathbb{C}^n$ if and only if its spectral radius $\rho(S)$ is such that $\rho(S) \leq 1$ and each eigenvalue $\lambda$ of $S$ such that $|\lambda| = 1$ has equal algebraic and geometric multiplicities.*

We observe now that, if the parameters are updated through relations (5), the sequence $M^k$ satisfies condition 1. above. Moreover, since the matrix $M$ represents the tensor-product of a univariate convergent subdivision scheme (see Remark 4), its eigenvalues $\lambda_i$ must necessarily satisfy $\lambda_1 = 1$ and $\lambda_i < 1$, $\forall i \neq 1$ (see e.g. [17]). In addition, the following theorem ensures that, if the matrix $M$ has 48 eigenvalues (counting with multiplicities) strictly smaller than one by modulo, then each matrix $M^k$ satisfies the hypothesis of Theorem 1 and thus is nonexpansive.

**Theorem 2.** *All the matrices $M^k$ are non expansive.*

*Proof.* We recall that, being $e = [1, 1, ..., 1]^T$, then $Me = e$ and $M^k e = e$, $\forall k$. Thus the matrices $M^k$ and $M$ have a common eigenvector $e$ with associated eigenvalue 1. Let $\lambda_1, \lambda_2, ..., \lambda_{49}$ be the eigenvalues of $M$ ordered by decreasing module, namely $|\lambda_1| \geq |\lambda_2| \geq ... \geq |\lambda_{49}|$. All eigenvalues are taken with their multiplicities. We know that $\lambda_1 = 1$. Similarly, for any matrix $M^k$, we denote by $\lambda_1^k, \lambda_2^k, ..., \lambda_{49}^k$ its eigenvalues, and $|\lambda_1^k| \geq |\lambda_2^k| \geq ... \geq |\lambda_{49}^k|$. Since 1 is an eigenvalue of $M^k$, it follows that $|\lambda_1^k| \geq 1$ for any $k$. Denote $q = |\lambda_2|$ and $q^k = |\lambda_2^k|$. Since eigenvalues continuously depend on the entries of matrices, it follows that $\lim_{k\to\infty} q^k = q$. Assume that $q < 1$. In this case there exists $N$ such that, for any $k > N$, we have $q^k < 1$, form which it follows $|\lambda_i^k| < 1, \forall i = 2, ..., 49$. Now, since 1 is an eigenvalue of $M^k$, it should necessarily be $1 = \lambda_1^k$ and as a consequence $\rho(M^k) = 1$, $\forall k > N$. □

The following theorem states that, given a sequence of matrices satisfying conditions 1. and 2., the refinement process (6) converges to a fixed point for $M$.

**Theorem 3.** *Let $\{M^k\}_{k=0}^{\infty}$ a sequence of matrices in $\mathbb{C}^{n\times n}$ that are non expansive with respect to the same vector norm $\| \quad \|$. Suppose also that*

$$\lim_{k\to\infty} M^k = M.$$

*Then, for any $x^0 \in \mathbb{C}^n$, the sequence*

$$x^{k+1} = M^k\, x^k, \quad k = 0, 1, 2, ... \tag{8}$$

*converges and in addition $\lim_{k\to\infty} x^k$ is a fixed point for $M$.*

*Proof.* Let $x^0 \in \mathbb{C}^n$ a vector. Since the matrix $M^k$ is non expansive, the sequence of iterates $\{x^k\}_{k>0}$ generated by the process (8) satisfies

$$\|x^{k+1}\| = \|M^k x^k\| \leq \|x^k\| \leq ... \leq \|x^0\|$$

i.e. it is a monotonic and bounded sequence and thus converges.

Let

$$\lim_{k\to\infty} x^k = \xi \tag{9}$$

its limit. We thus need to prove that $\xi$ is a fixed point of $M$. To this aim, we have

$$\lim_{k\to\infty} \{M\xi - M^k x^k\} = \lim_{k\to\infty} \{(M - M^k)\xi + M^k(\xi - x^k)\} = 0$$

and therefore $\lim_{k\to\infty} M^k x^k = M\xi$. This last relation, together with (9) implies $M\xi = \xi$. □

If we now indicate with $e$ the vector $e = [1, 1, ..., 1]^T$, from (7) we see that $\lambda = 1$ is an eigenvalue of $M$. Moreover, from (3) and (4) it can be easily verified that for any parameters configuration the rows of $M$ sum to one, and as a consequence the null space of $I - M$ is generated by $e$ (here $I$ is the identity matrix). By Theorem 3, the limit of the sequence of iterates generated by the refinement process in the neighborhood of $p_0^0$ belongs to the space generated by $e$. Moreover, since $p_0^0$ is a fixed point of the iterative process, we can conclude that all the initial points in the neighborhood of $p_0^0$ converge to $p_0^0$ as $k \to \infty$.

As a concluding remark, we let the reader notice that the presented analysis method allows us to prove convergence for any given subdivision scheme. As discussed, the chosen parameters updating strategy makes it easy to verify that conditions 1. to 3. are satisfied, thus, in this setting, any subdivision scheme converges to a continuous limit surface. Using a different parameters updating method implies proving that conditions 1. to 3. hold, which is in general possible but not trivial.

## 5. Numerical results

In this section we present some numerical experimentation about the NULISS subdivision scheme. Our tests have two main purposes: 1) examine the quality of NULISS surfaces and compare it with other non uniform interpolation methods, 2) conjecture that, if the reference scheme is $C^1$, the limit surfaces generated by NULISS are $G^1$ continuous.

*5.1. Surface quality*

The surfaces shown in the following figures have been generated using the scheme 1 as reference scheme, with centripetal parameterization and, if open, through linear extrapolation along the cross-boundary direction. We start with two simple, yet effective examples. We modified the regular torus mesh, so as to obtain an initial mesh whose section curves have corresponding edges of remarkably different lengths (Fig. 8 (a)). In such meshes, the uniform parameterization introduces a significant distortion with respect to the parameterization of the individual initial section polylines. As a consequence an unwanted artifact appears in the limit surface of the uniform scheme (Fig. 8 (b) and (d)), which is not present in the NULISS surfaces generated from the same initial meshes (Fig. 8 (c) and (e)). The kind of artifact highlighted by this example is particularly evident if we look at one section curve of the uniform and NULISS limit surfaces as illustrated in Fig. 9 for the upper-row mesh. While in the uniform case each section curve has the same parameterization in both directions, in the latter one each section curve maintains its own (centripetal) parameterization.

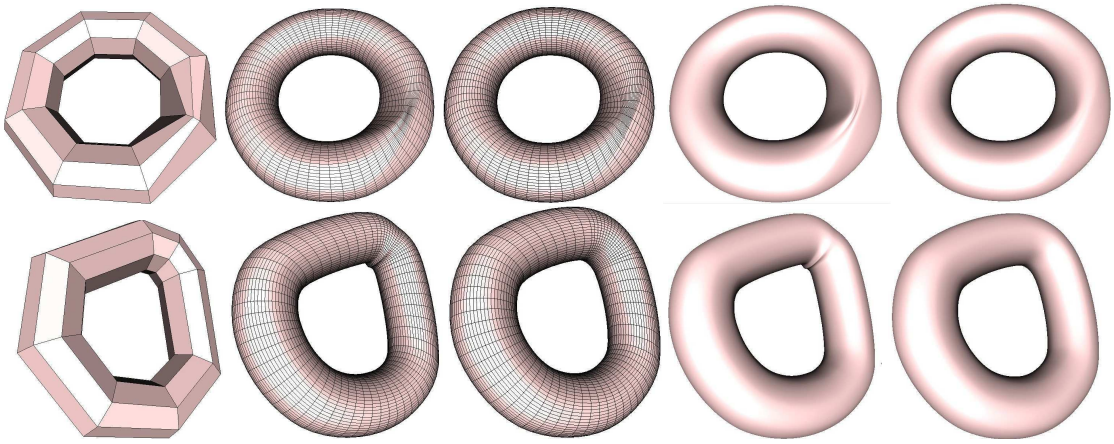

(a) Initial mesh (b) Uniform, 3 steps (c) NULISS, 3 steps (d) Uniform limit (e) NULISS limit

Figure 8: Comparison between uniform tensor product bicubic spline surface and NULISS.

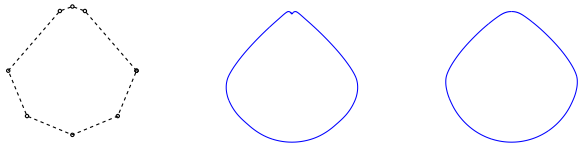

(a) (b) (c)

Figure 9: Starting polyline corresponding to a section of the initial mesh on the top row of Figure 8 (a) ; Corresponding section curve of the uniform subdivision surface (b) and of NULISS (c).

To give a general idea of the quality of the NULISS surfaces, we provide in Figure 10 the results that we got by applying NULISS to a variety of initial meshes. The lamp mesh is obtained by revolution of a profile curve with extremely short and long edges, and thus it is essentially uniform in one grid direction and highly non uniform in the other. The middle row mesh represents the upper part of a fire hydrant, it is not a revolution surface and it evidently presents highly non uniform section curves in both grid directions. Finally, the vase mesh is obtained by scaled versions of one section curve, shifted along the vertical axis with long and short shift steps. The considered meshes are

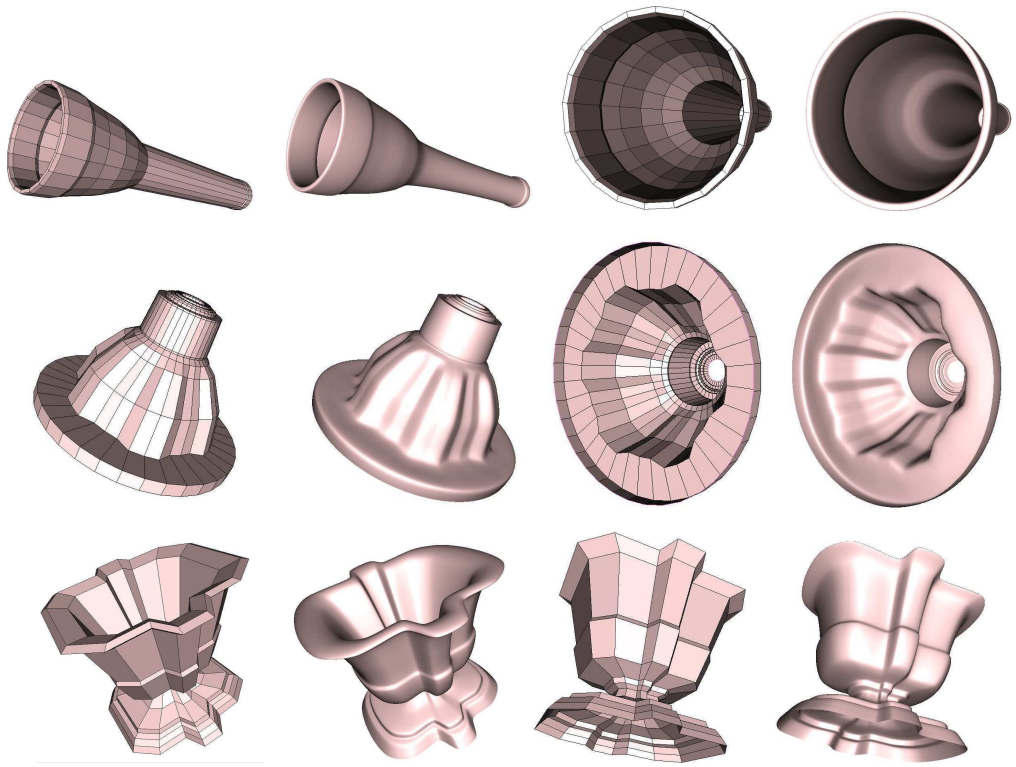

Figure 10: NULISS surfaces and the related initial meshes.

characterized by highly non uniform initial section polylines, so that the uniform scheme fails on all of them.
We have also tested NULISS on a wide set of data, acquired through a needle scanning device. We have reconstructed the data by means of NULISS and non uniform tensor product bicubic spline surfaces. As shown in Figure 11 NULISS gives us a faithful reconstruction, preserving the details present in the data. Oppositely, in some areas - see e.g. along the top border of the wings or top of head - tensor product splines generate more undulations than the ones present in the acquired data.
Finally, an application of the NULISS subdivision scheme was presented in [2]. In that work, the NULISS subdivision scheme was used to generate a surface starting from some of its feature curves, acquired through an interactive pen-like device. While the user interactively scans the feature curves, the surface underneath needs to change accordingly, so, in such a situation, it is fundamental to have at disposal a quick method that at the same time allows for updating the surface shape and interpolating all the given data with satisfactory quality. In the time of the work presented in [2], although NULISS proved to be optimal on the side of surface behavior, none of its analytic properties were known, especially it was not clear whether the limit surfaces were continuous for any parameters configuration.

### *5.2. $G^1$ continuity*

In Section 4 it was proved that the NULISS scheme generates continuous limit surfaces for any set of initial parameters, supposed that the associated reference scheme generates at least continuous limit curves. Moreover, analyzing the pattern of knot intervals through the successive refinements, it was shown that away from the boundary of each initial face, the knot vectors can be scaled to uniform; thus, if the reference scheme is $C^1$, NULISS will generate a $C^1$ limit surface in the interior of each initial face. Around the border of an augmented face, $G^1$ continuity can be only conjectured and proven by numerical testing.

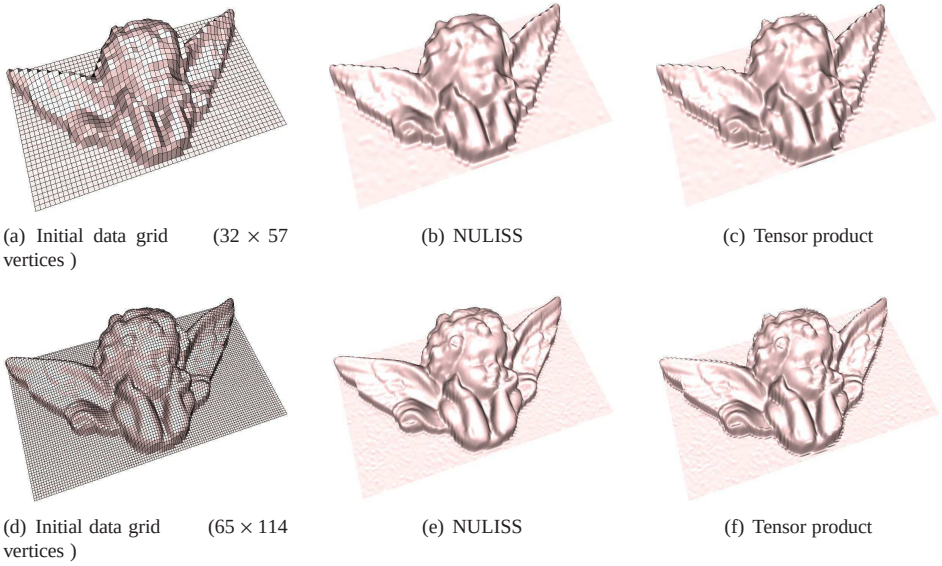

(a) Initial data grid ($32 \times 57$ vertices ) (b) NULISS (c) Tensor product

(d) Initial data grid ($65 \times 114$ vertices ) (e) NULISS (f) Tensor product

Figure 11: Reconstruction of scanned data through NULISS and non uniform cubic tensor product splines.

Without loss of generality, we can confine our analysis to the neighborhood of one of the initial vertices, which is at the intersection of four augmented faces. The limit surface has a tangent plane at the considered vertex if it is regular in the neighborhood of the vertex and the normals to the four faces meeting at it converge in the limit to a unique normal vector. Thus we have verified that the maximum angle between the normals to the four faces meeting at a prescribed vertex tends to 0 as the subdivision level $k$ goes to infinity.
The normal vector to each face is computed by splitting each face into two triangles, the first of them determined by the examined vertex and the two adjacent vertices of the face and the second being its obvious complimentary. The face normal vector is then obtained by averaging the normals to these two triangles.
We performed the above numerical analysis considering a wide variety of meshes, analyzed around vertices with different local configurations of surrounding points. We used as reference scheme for NULISS both schemes with coefficients (1) and (2) and all the numerical tests indicate convergence of normals, confirming the conjecture that the NULISS scheme be $G^1$.
An example of the results obtained through the proposed analysis is given in Table 1, where we have considered the meshes in Figure 8. We chose the test vertices are among those vertices that are surrounded by augmented faces and refined the meshes with the uniform subdivision scheme, which is known to generate everywhere $C^1$ limit surfaces, and with NULISS. Table 1 compares the maximum angles $\theta_{max}$ (in radians) between the normals to the four faces meeting at the selected vertices at the first 25 subdivision levels.
In the case of NULISS, $\theta_{max}$ progressively decreases to zero and, at the same subdivision step $k$, its values have the same (or lower) magnitude order as those of the corresponding uniform setting. We also computed the maximum distance $\delta_{max}$ from the considered vertex and the vertices in its one neighborhood. As proven analytically in Section 4 this distance tends to zero as $k$ tends to infinity; in addition the following tables show that the convergence rate in the case of NULISS is similar to that of the uniform scheme.

## 6. Summary and future work

Non-uniform tensor-product interpolants often give rise to significant undulation artifacts, due to the strict structure of the underlying parameterization. For this reason, the centripetal parameterization, that is proven to be optimal in the univariate case, does not significantly improve the visual appearance of the surface in the tensor-product bivariate setting.

Table 1: Numerical analysis in the neighborhood of selected test vertices. Numbers on the edges represent the initial knot intervals computed according to the centripetal parameterization. The red circle indicates the vertex taken into exam.

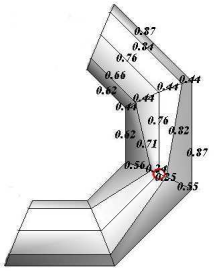


| | TP uniform | | NULISS augmented | |
|---|---|---|---|---|
| $k$ | $\theta_{max}$ | $\delta_{max}$ | $\theta_{max}$ | $\delta_{max}$ |
| 3 | 7.58889e-01 | 7.50140e-02 | 3.26623e-02 | 7.50736e-02 |
| 5 | 3.84622e-01 | 1.83510e-02 | 2.62558e-02 | 1.83898e-02 |
| 10 | 2.52885e-02 | 5.69647e-04 | 2.10802e-03 | 5.71154e-04 |
| 15 | 1.19628e-03 | 1.77983e-05 | 1.05870e-04 | 1.78457e-05 |
| 20 | 5.00678e-05 | 5.56193e-07 | 4.55890e-06 | 5.57675e-07 |
| 25 | 1.98420e-06 | 1.73810e-08 | 2.14908e-07 | 1.74273e-08 |

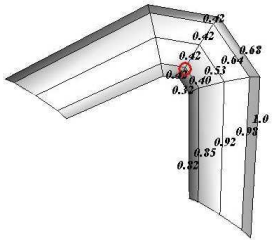


| | TP uniform | | NULISS augmented | |
|---|---|---|---|---|
| $k$ | $\theta_{max}$ | $\delta_{max}$ | $\theta_{max}$ | $\delta_{max}$ |
| 3 | 1.18652e+00 | 2.42100e-02 | 1.60553e-01 | 2.53548e-02 |
| 5 | 5.91877e-01 | 5.89203e-03 | 4.39939e-02 | 6.32675e-03 |
| 10 | 3.97887e-02 | 1.83151e-04 | 1.81903e-03 | 1.97671e-04 |
| 15 | 1.89073e-03 | 5.72337e-06 | 7.42709e-05 | 6.17722e-06 |
| 20 | 7.93129e-05 | 1.78855e-07 | 2.91541e-06 | 1.93038e-07 |
| 25 | 3.07538e-06 | 5.58923e-09 | 1.89074e-07 | 6.03244e-09 |

In this paper, we have presented a novel class of non-uniform local interpolatory subdivision surfaces that generalize the family of non-uniform interpolatory 4-point schemes to quadrilateral meshes. This new proposal generates limit surfaces with a better visual appearance than the well-established tensor-product (spline) representation. To a large extent, the advantage of this new construction is that the whole local parameterization is used, instead of a global average of the parameters. One of the consequences of this flexibility with respect to the parameterization, is that each section curve is interpolated together with its parameters, thus maintaining its own centripetal parameterization.
The resulting limit surfaces are $C^0$-continuous and proving $C^1$ continuity will be one of our future research objectives. Another challenge would be finding a parameterization algorithm for NULISS surfaces, in such a way that they will become fully comparable with interpolation methods based on non uniform splines. Another step forward will be the generalization of the proposed edge and face point rules to meshes with extraordinary vertices. We believe that the advantages of a non-uniform parameterization would be significant also when interpolating meshes of arbitrary topology.


### Acknowledgements

The authors thank Nira Dyn and Michael Floater for useful discussions and suggestions.


### References


[1] Beccari, C.V., Casciola, G., Romani, L., 2010. Non-uniform interpolatory curve subdivision with edge parameters built-upon compactly supported cardinal splines. Submitted for publication.

[2] Beccari, C.V., Farella, E., Liverani, A., Morigi,S., Rucci, M., 2010. A fast interactive reverse engineering system. Computer-Aided Design 42(10), 860-873.

[3] Cashman, T.J., Dodgson, N.A., Sabin, M.A., 2009. A symmetric, non-uniform, refine and smooth subdivision algorithm for general degree B-splines. Comput. Aided Geom. Design 26(1), 94-104.

[4] Catmull, E., Clark, J., 1978. Recursively generated B-spline surfaces on arbitrary topological meshes. Computer-Aided Design 10(6), 350-355.

[5] Dahmen, W., Goodman, T.N.T., Micchelli, C.A., 1988. Compactly supported fundamental functions for spline interpolation. Numer. Math. 52, 639-664.

[6] Daubechies, I., Guskov, I., Sweldens, W., 1999. Regularity of irregular subdivision. Constr. Approx. 15(3), 381-426.

[7] Dyn, N., Floater, M., Hormann, K., 2009. Four-point curve subdivision based on iterated chordal and centripetal parameterizations. Comput. Aided Geom. Design 26(3), 279-286.
[8] Dyn, N., Levin, D., 1995. Analysis of asymptotically equivalent binary subdivision schemes. J. Math. Anal. Appl. 193, 594-621.
[9] Handbook of Computer Aided Geometric Design, Gerald Farin, Josef Hoschek, Myung-Soo Kim, Eds. Elsevier, 2002.
[10] Floater, M., 2008. On the deviation of a parametric cubic spline interpolant from its data polygon. Comput. Aided Geom. Design 25(3), 148-156.
[11] Grohs, P, 2008. Smoothness analysis of subdivisions schemes on regular grids by proximity. SIAM Journal on Numerical Analysis 46(4), 2169-2182.
[12] Horn, R.A., Johnson, C.R., 1985. Matrix Analysis, Cambridge University Press, Cambridge, UK.
[13] Müller, K., Reusche, L., Fellner, D., 2006. Extended subdivision surfaces: Building a bridge between NURBS and Catmull-Clark surfaces. ACM Transactions on Graphics 25(2), 268-292.
[14] Sederberg, T.W., Zheng, J., Sewell, D., Sabin, M., 1998. Non-uniform recursive subdivision surfaces. Proceedings of the 25th annual conference on Computer Graphics and Interactive Techniques, pp. 387-394.
[15] Wallner, J., Dyn, N., 2005. Convergence and $C^1$ analysis of subdivision schemes on manifolds by proximity. Comput. Aided Geom. Design 22, 593-622.
[16] Wallner, J., 2006. Smoothness analysis of subdivisions schemes by proximity. Constr. Approx. 24(3), 289-318.
[17] Warren, J., Weimer, H., 2002. Subdivision Methods for Geometric Design: A Constructive Approach. Morgan Kaufmann.
[18] Yuksel, C., Schaefer, S., Keyser, J., 2009. On the parameterization of Catmull-Rom curves. Proceedings of ACM Joint Conference on Geometric and Physical Modeling, pp. 47-53.
[19] Zorin, D., 2000. A method for analysis of $C^1$-continuity of subdivision surfaces. SIAM J. Numer. Anal. 37(5), 1677-1708.